Supporting materials

Interface Engineering of Highly Stable CeO_2/CoFe@C Electrocatalysts for Synergistically Boosting Overall Alkaline Water Splitting Performance

Waleed Yaseen[a,1], Karim Harrath[b,1], Guangya Li[a], Bashir Adegbemiga Yusuf[a], Suci Meng[a*], Meng Xie[a], Iltaf Khan[c], Jimin Xie[a,d], Changkun Xia,[a] Yuanguo Xu[a*]

[a]School of Materials Science & Engineering, School of Chemistry and Chemical Engineering, School of Pharmacy, Jiangsu University, Zhenjiang 212013, China

[b] Fundamental Science Center of Rare Earths, Ganjiang Innovation Academy, Chinese Academy of Sciences, Ganzhou 341000, China

[c]School of Environmental & Chemical Engineering Jiangsu University of Science and Technology Zhenjiang 212003, PR China

[d]Jiangsu Jiangke Graphene Research Institure Co., LTD, Jiangsu Jiangke Composite Material Co., LTD

*Corresponding authors: Suci Meng (mengsc@ujs.edu.cn), Yuanguo Xu (xuyg@ujs.edu.cn)

[1]These authors contributed equally to this work

1.1 Calibration of Hg/HgO reference electrodes to RHE potential

The reference electrodes were calibrated within a conventional three-electrode cell system, wherein the flame-annealed Pt foil served as both the working and counter electrode, and Mercury/mercury oxide (Hg/HgO) functioned as the reference electrode in 1.0 M KOH at 25 °C. Before the electrode calibration, high-purity H_2 gas was purged into the electrolyte solution for 25 minutes to eliminate impurities. The linear sweep voltammetry (LSV) curve was generated with a scan rate of 5 mV s^{-1}, and the zero current was established as the thermodynamic potential for the Hydrogen Evolution Reaction (HER). The findings revealed that at zero current, the potential intersecting at that point was considered the thermodynamic potential for HER at a specific pH. Consequently, all recorded potentials were normalized using the formula $E_{(RHE)} = E_{Hg/HgO}+0.921$ (1.0 M KOH, pH=14), as illustrated in Fig S1(a-b).

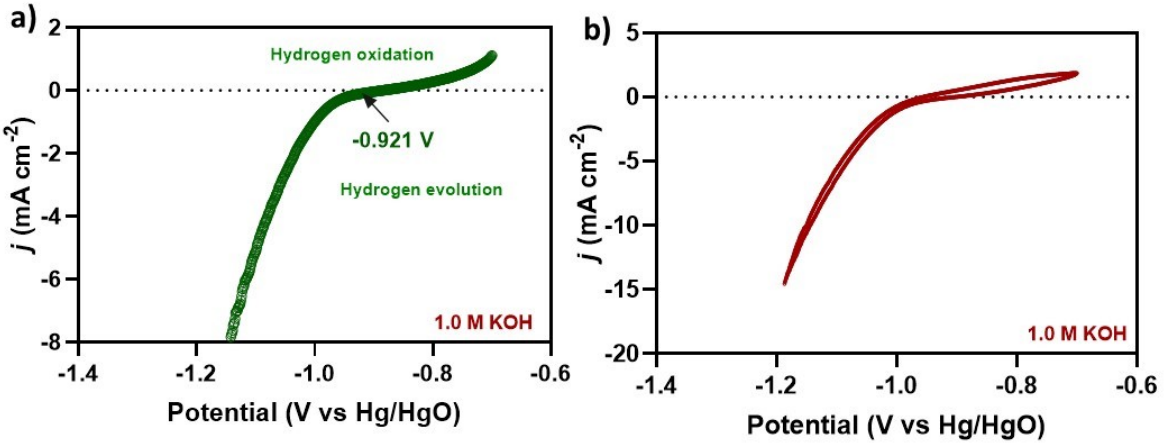

Fig. S1. (a) LSV polarization calibration curves of Hg/HgO reference electrode in 1.0 M KOH; and (b) Corresponding CV curves in 1.0 M KOH.

1.2 Faradaic Efficiency and H_2/O_2 volume calculations

The Faradaic efficiency was determined by analyzing the overall quantity of generated H_2 and O_2 alongside the total charge (Q) transmitted through the electrolytic cell. The water drainage method measured the total volume of H_2/O_2 produced. Afterwards, a constant current density of 100 $mAcm^{-2}$ was applied for a certain period. Assuming the production of one O_2 and H_2 molecule requires four electrons and two electrons, respectively [1,2].

Step 1: Calculate the charge

$$Q = I * t$$

Q is the charge in coulombs (C), I is the current in amperes (A), and t is the time in seconds (s)

Step 2: Calculate the moles of hydrogen and oxygen

$$n = Q / (2 * F) \text{ for } H_2$$
$$n = Q / (4 * F) \text{ for } O_2$$

F is the Faraday constant in coulombs per mole (96485 C/mol)

Step 3: Calculate the volume of hydrogen and oxygen gas

$$V_{H_2} = n\,(H_2) * Vm$$
$$V_{O_2} = n\,(O_2) * Vm$$

The molar volume (Vm) is the volume occupied by one mole of gas at standard temperature and pressure (STP). STP is 0°C (273.15 K) and 1 atmosphere (101,325 Pa). The molar volume of a gas at STP is approximately 22.4 L/mol.

Step 4: Faradaic efficiency calculation

Faradaic efficiency of water splitting catalyzed by $Ce_{20}CoFe@C/750$ was calculated by dividing the amount of the experimentally produced gas by the theoretical amount of gas, which is calculated by the charge passed through the electrode:

$$FE\,(H_2,\%) = \frac{V\ experiment}{V\ theoretical} X\ 100\% = \frac{V\ experiment}{[(2/4) * (Q/F) * Vm} X\ 100\% \quad \text{for HER}$$

$$FE\,(H_2,\%) = \frac{V\ experiment}{V\ theoretical} X\ 100\% = \frac{V\ experiment}{[(1/4) * (Q/F) * Vm} X\ 100\% \quad \text{for OER}$$

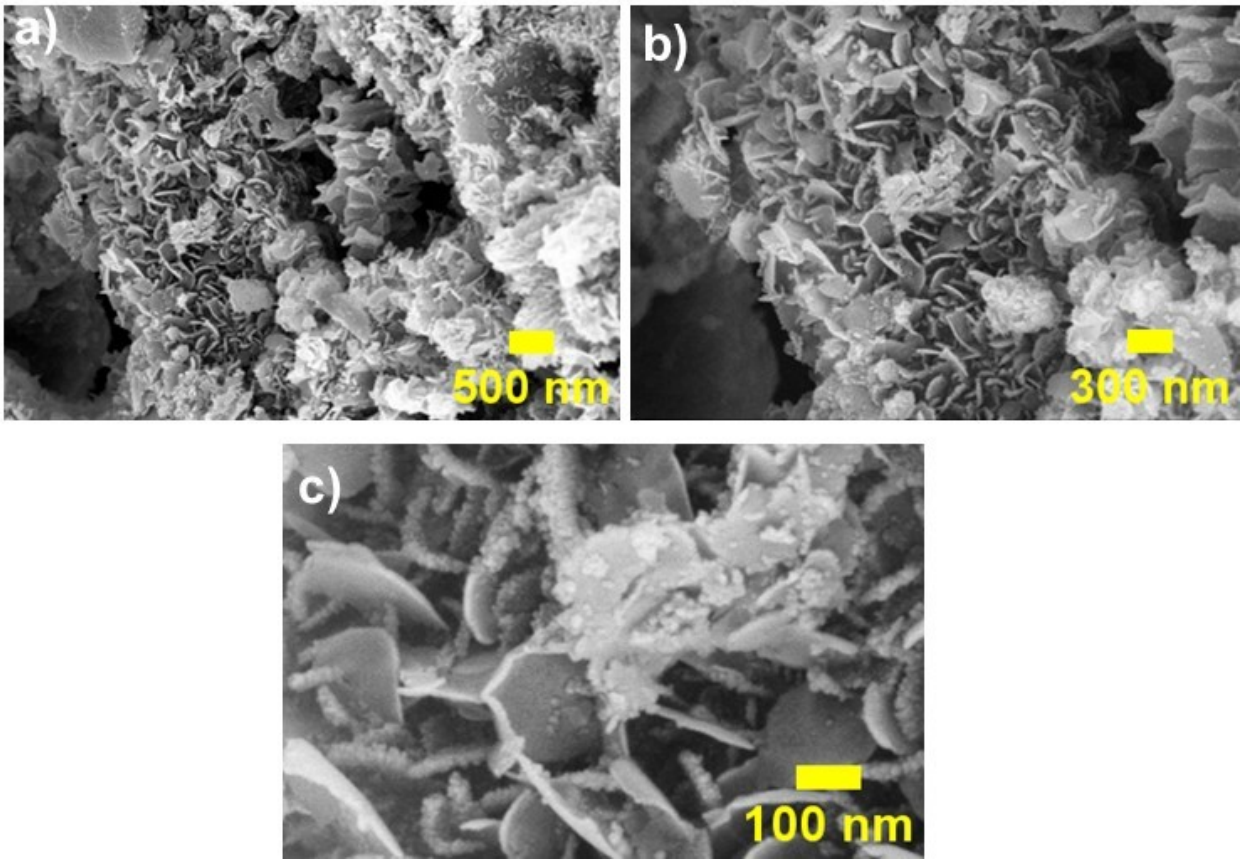

Fig. S2. (a-c) SEM images of CoFe@C/750 sample.

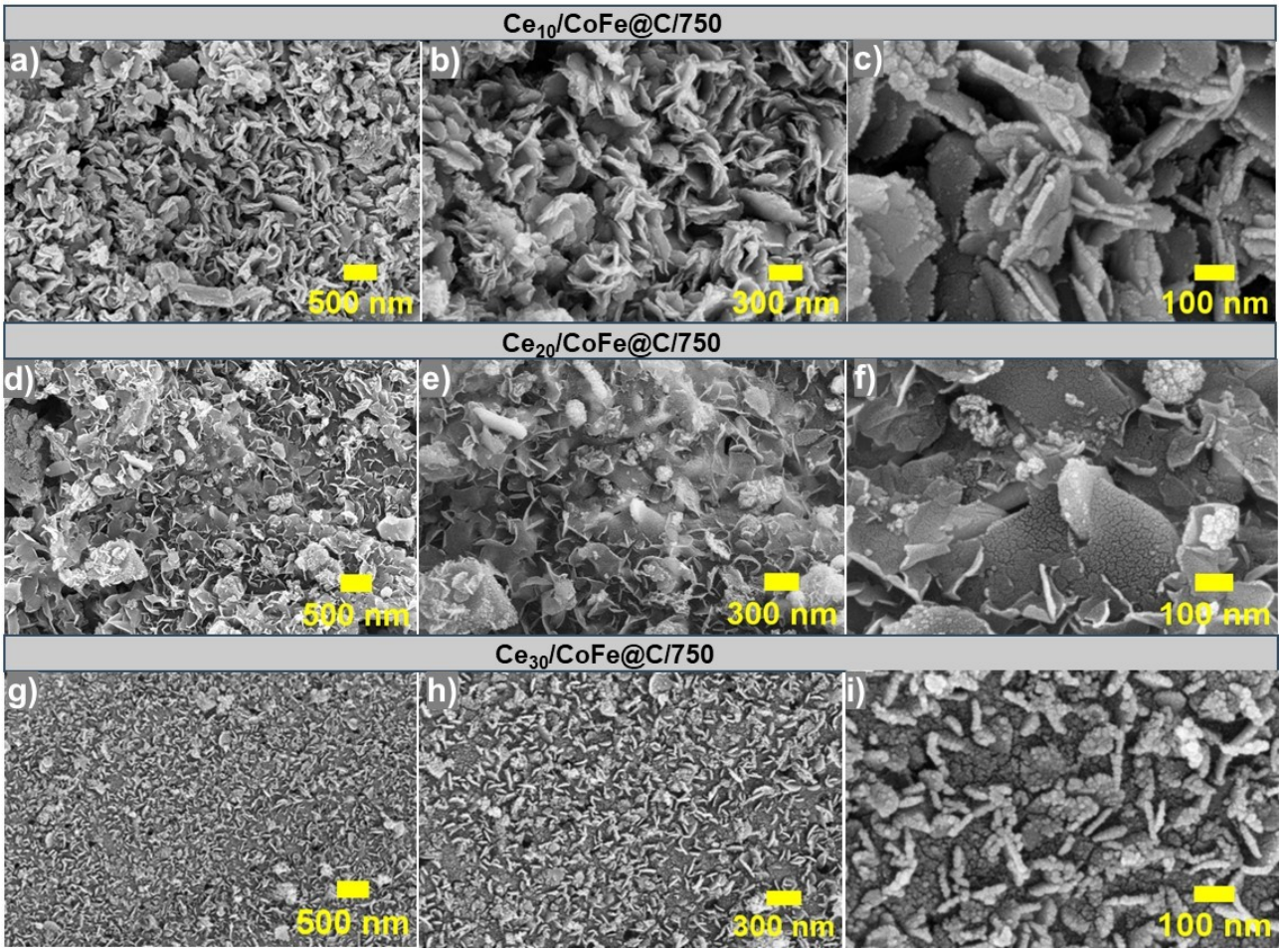

Fig. S3. SEM images of as-prepared catalyts (a-c) Ce_{10}/CoFe@C/750, (d-f) Ce_{20}/CoFe@C/750, and (g-i) Ce_{30}/CoFe@C/750.

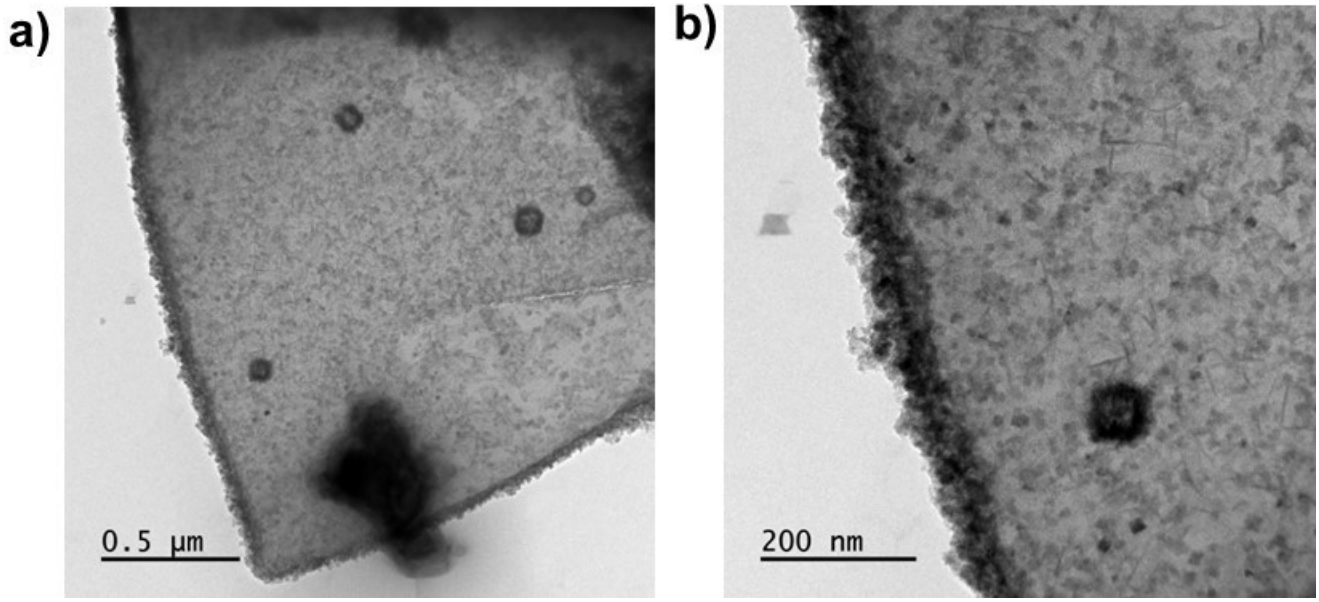

Fig. S4. (a-b) High-resolution and low-resolution TEM images of the Ce_{20}/CoFe@C/750 sample.

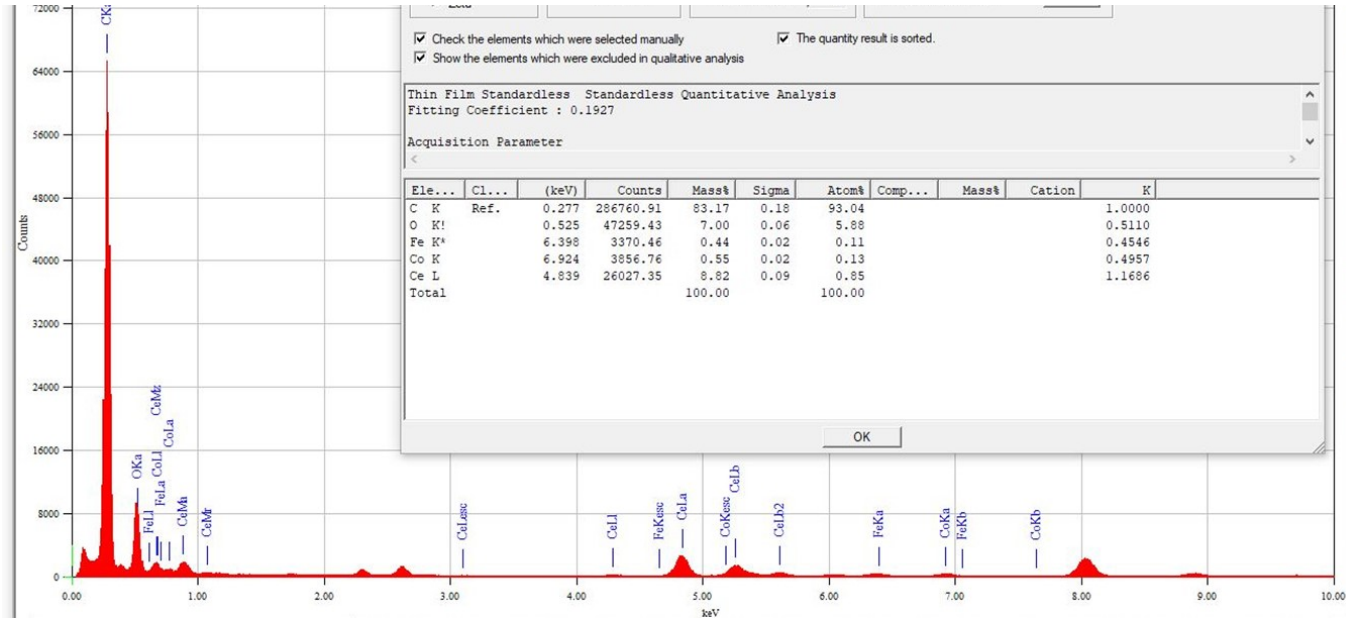

Fig. S5. EDS spectrum obtained via TEM, illustrating the elemental composition of the Ce_{20}/CoFe@C/750 sample.

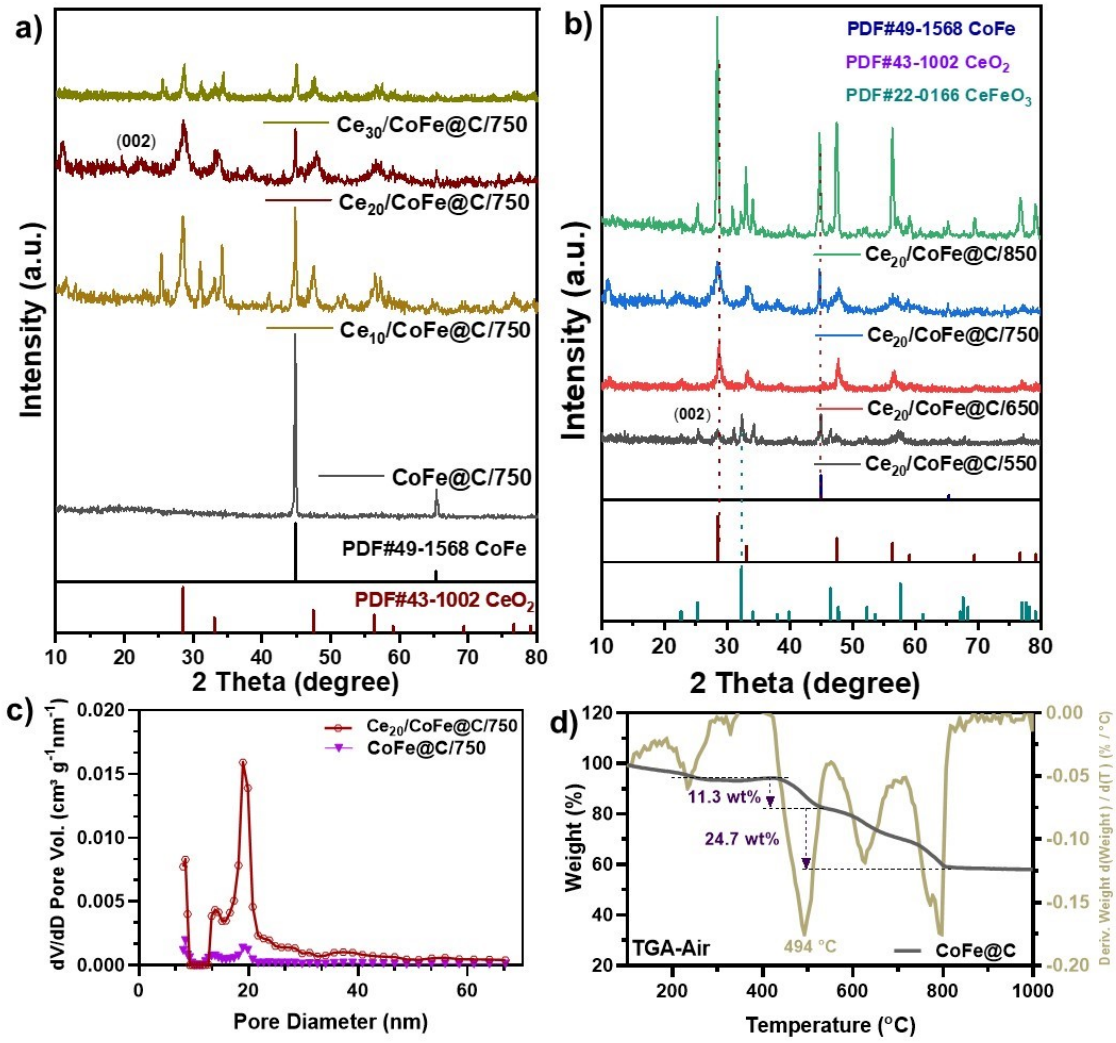

Fig. S6. (a) XRD pattern of the as-prepared samples with different Ce wt.%, (b) XRD pattern of the as-prepared samples at different temperatures, (c) Pore size distribution of CoFe@C/750 and Ce_{20}/CoFe@C/750 sample, and (c) DSC-TGA plot for CoFe@C/750 sample.

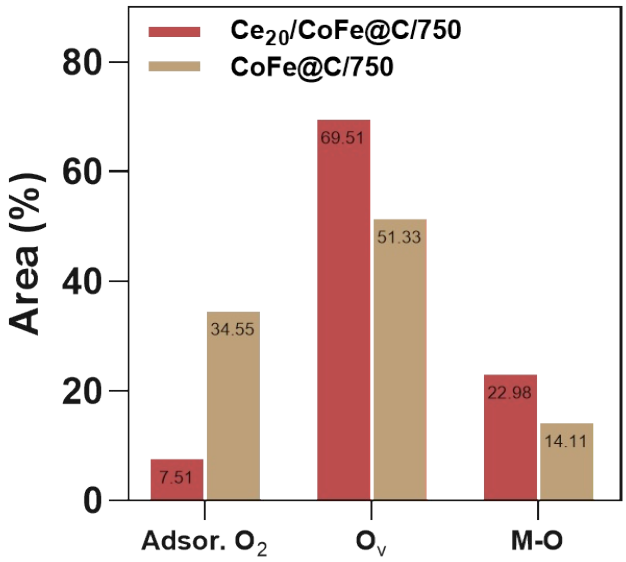

Fig. S7. Comparison of relative peak areas in O 1s spectra for Cc_{20}/CoFe@C/750 and CoFe@C/750 samples.

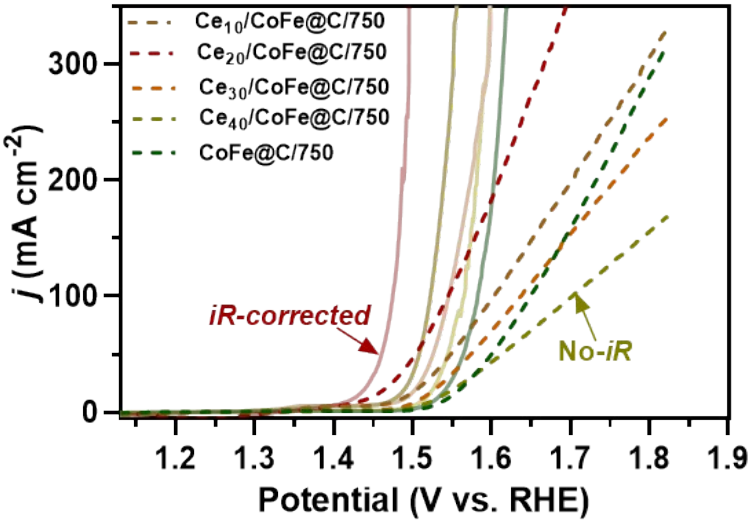

Fig. S8. *iR*-corrected and non-*iR*-corrected LSV curves of the prepared samples.

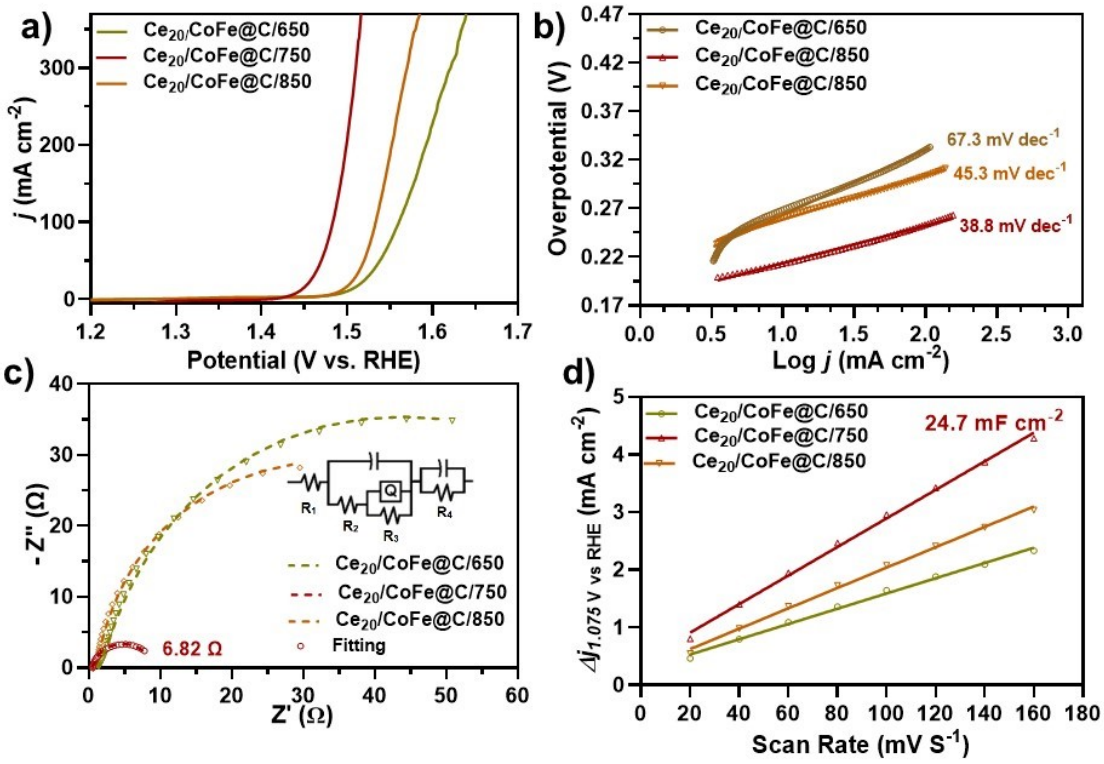

Fig. S9 (a) LSV curves of samples prepared at different temperatures, (b) Tafel slopes; and (c) EIS inset: equivalent circuit model for fitting the Nyquist plots (d) C_{dl} measurement of Ce_{20}/CoFe@C/650, Ce_{20}/CoFe@C/750, and Ce_{20}/CoFe@C/850 samples.

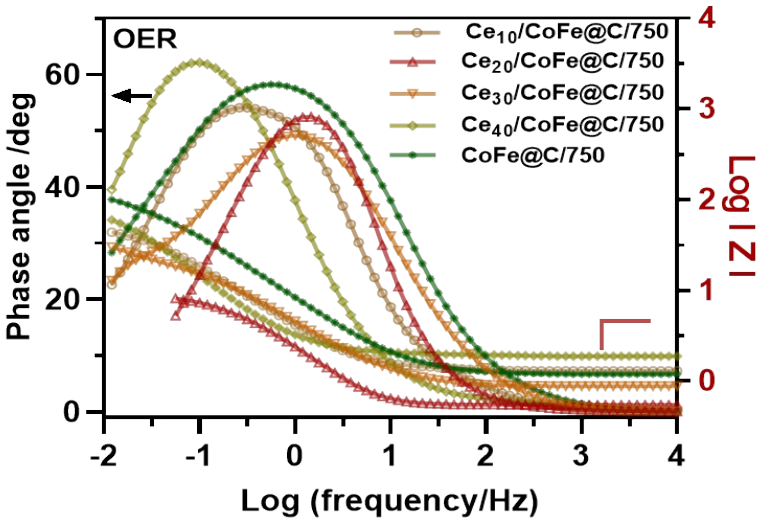

Fig. S10. Bode plot for EIS measurement, showing the frequency response of the system with magnitude and phase data across a range of frequencies.

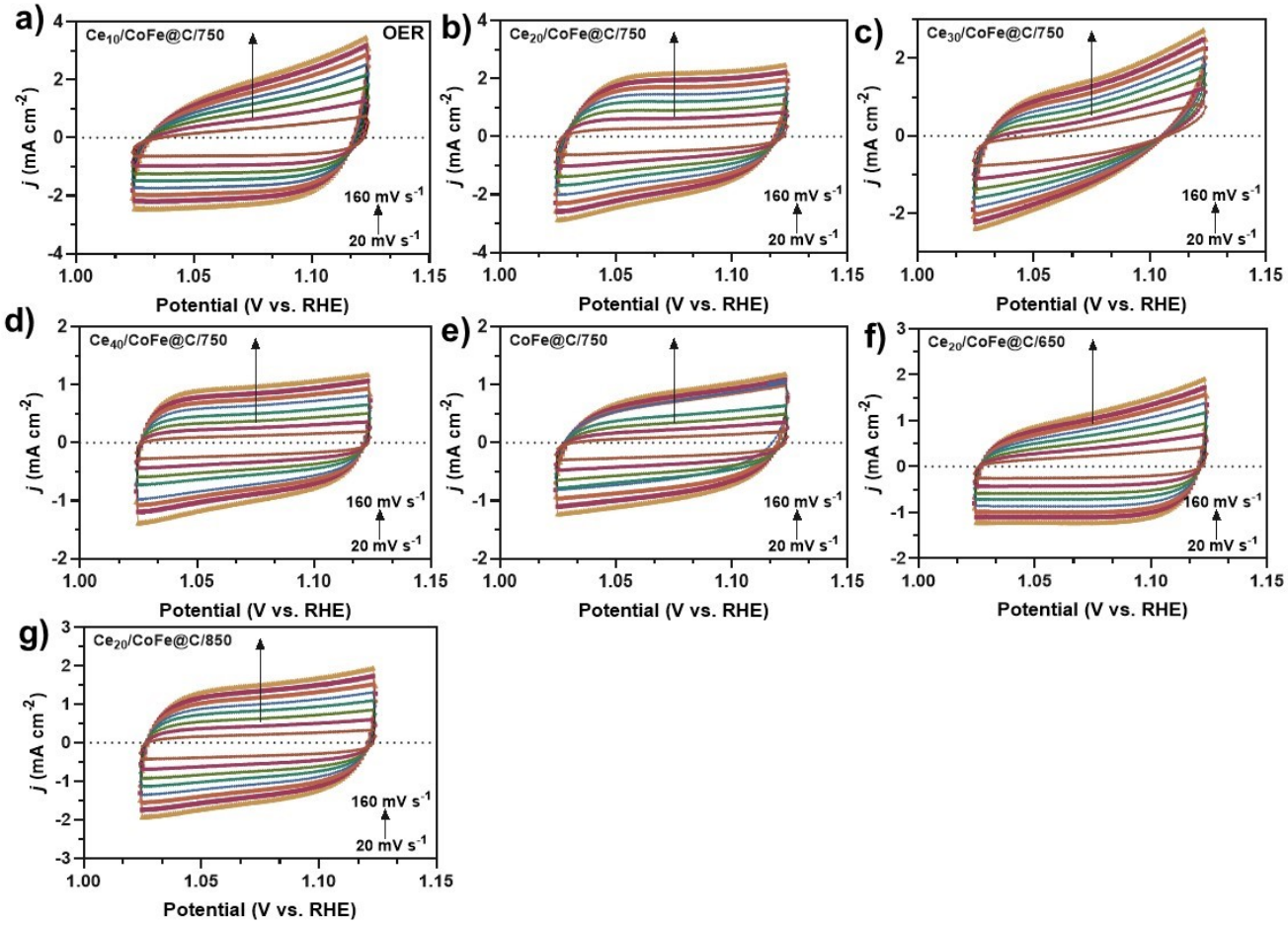

Fig. S11. CV at different scan rates from 20 to 160 mV s^{-1} for OER in 1.0 M KOH solution. (a) Ce_{10}/CoFe@C/750, (b) Ce_{20}/CoFe@C/750, (c) Ce_{30}/CoFe@C/750, (d) Ce_{40}/CoFe@C/750, (e) CoFe@C/750, (f) Ce_{20}/CoFe@C/650, and (g) Ce_{20}/CoFe@C/850.

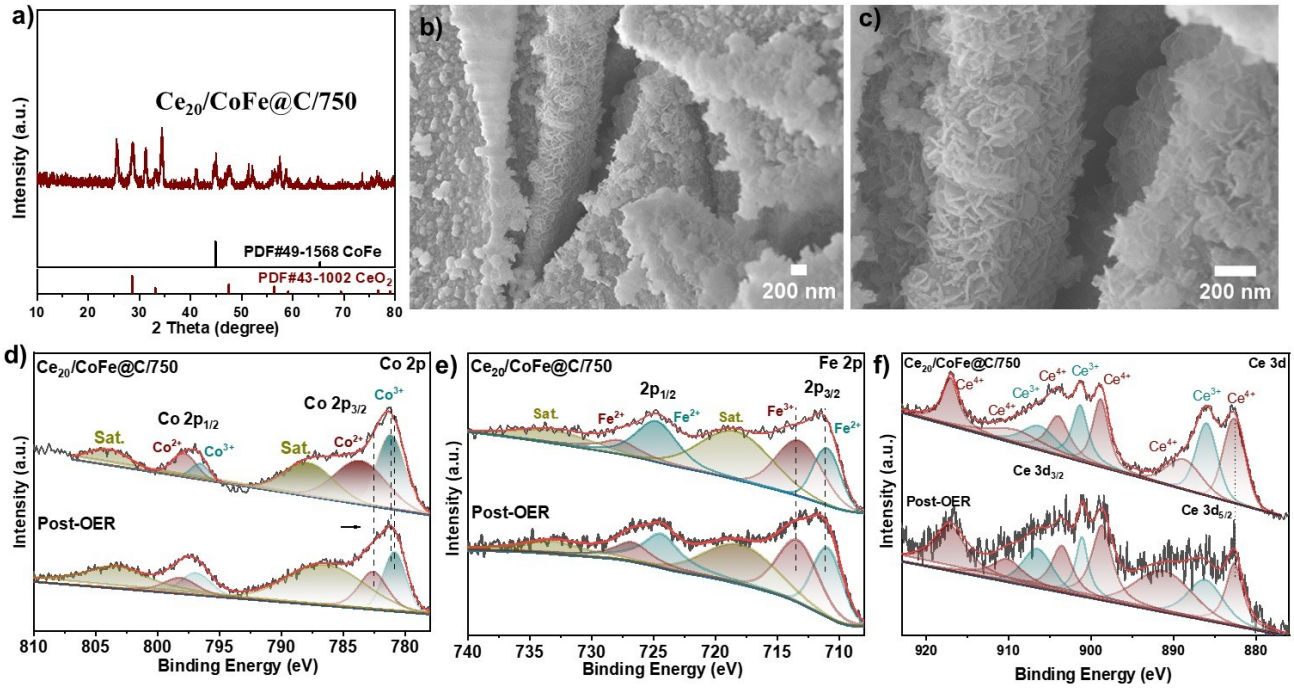

Fig. S12. (a) Post-OER XRD results of Ce_{20}/CoFe@C/750 sample, (b-c) SEM images results of post-OER stability of Ce_{20}/CoFe@C/750 sample, and d-f) Post OER XPS analysis of Ce_{20}/CoFe@C/750 sample.

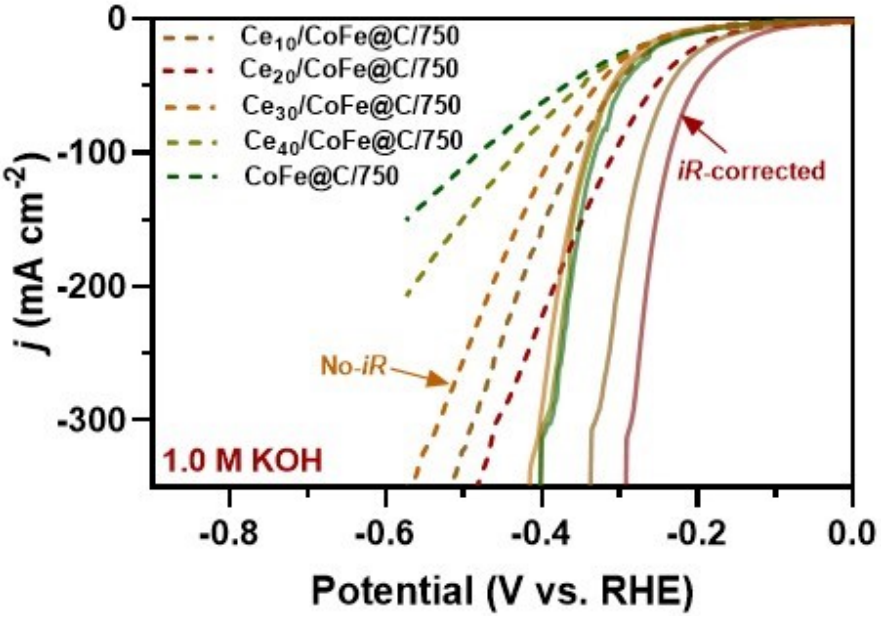

Fig. S13. *iR*-corrected and non-*iR*-corrected LSV curves of the as-prepared samples.

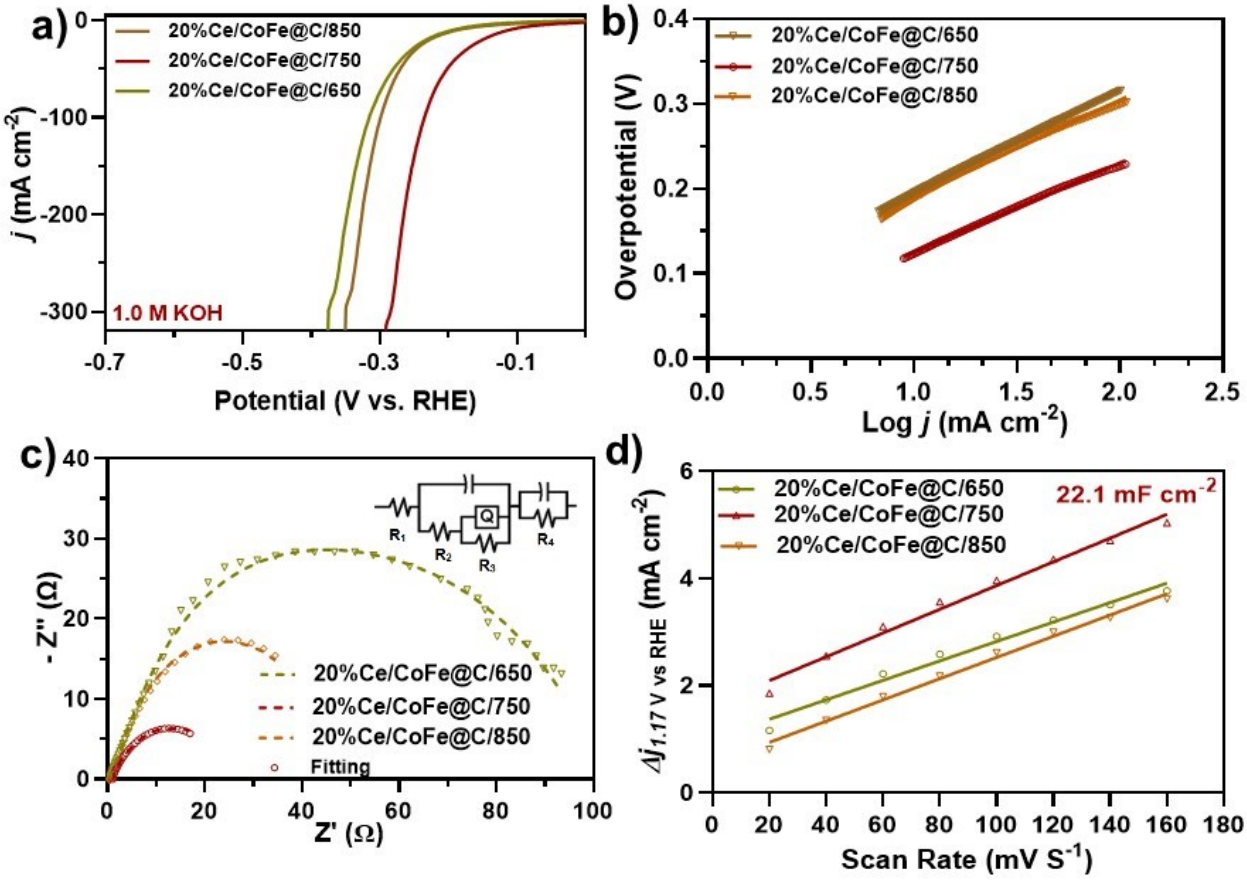

Fig. S14. (a) LSV curves of samples prepared at different temperatures, (b) Tafel slopes; and (c) EIS inset: equivalent circuit model for fitting the Nyquist plots (d) C_{dl} measurement of Ce_{20}/CoFe@C/650, Ce_{20}/CoFe@C/750, and Ce_{20}/CoFe@C/850 samples.

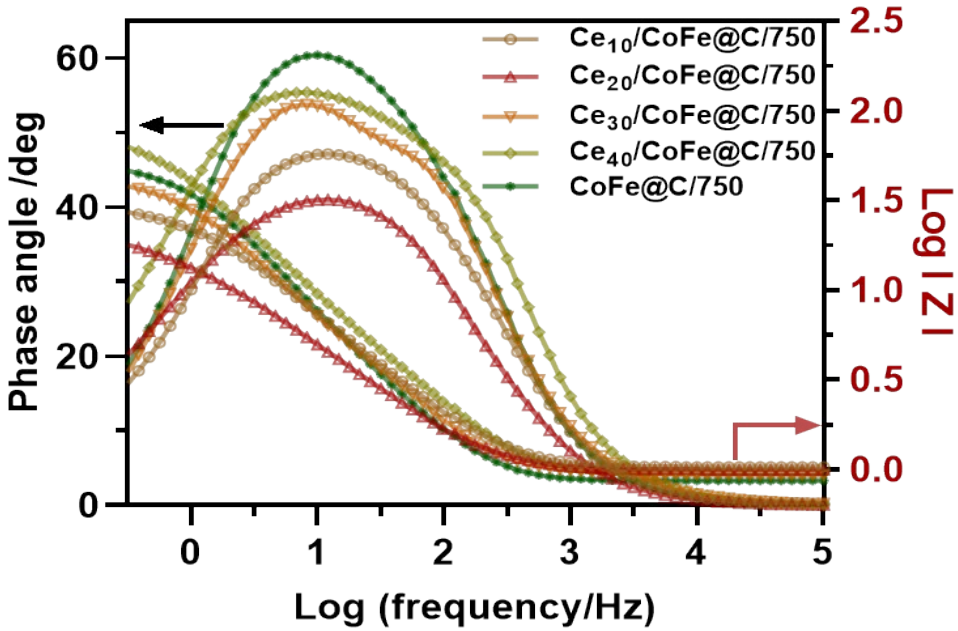

Fig. S15. Bode plot for EIS measurement, showing the frequency response of the system with magnitude and phase data across a range of frequencies.

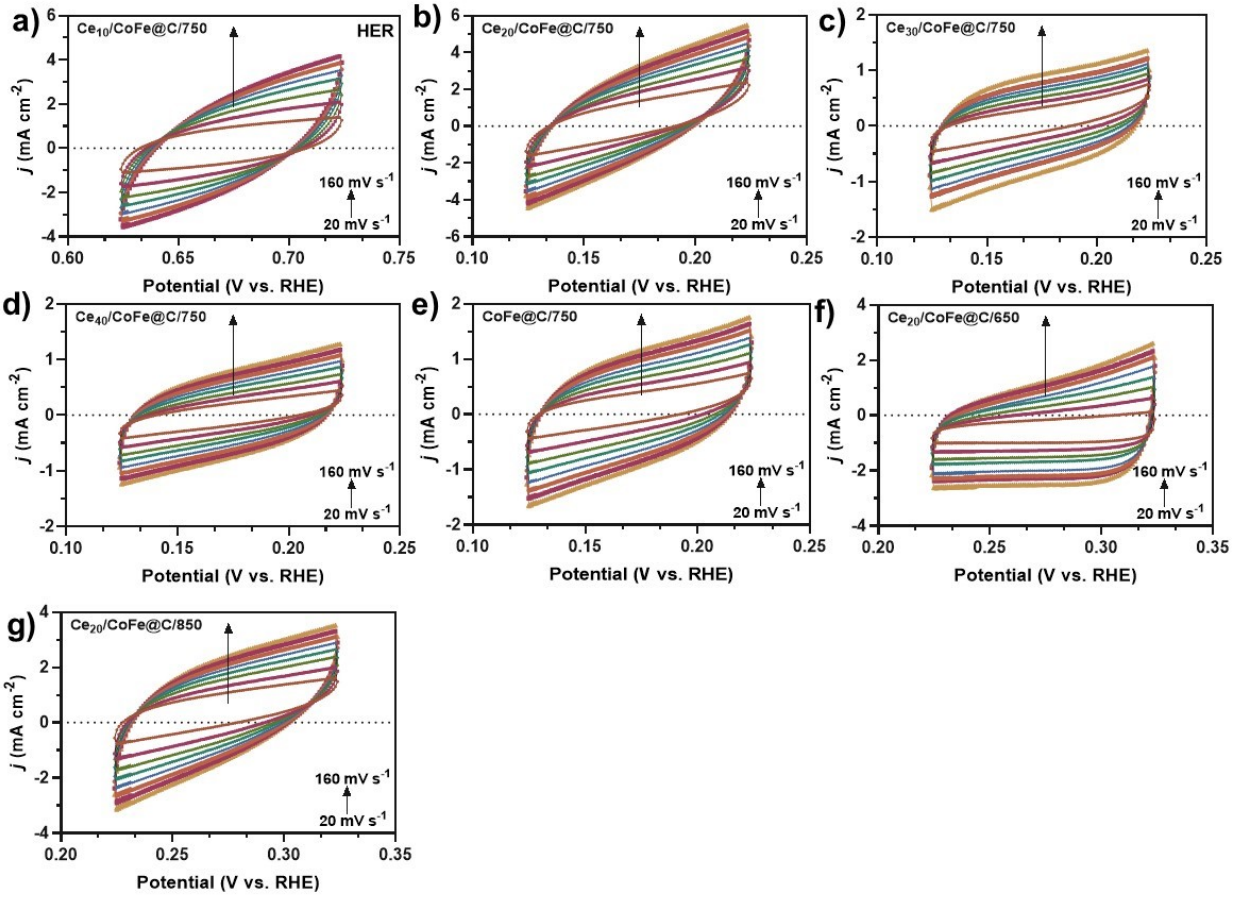

Fig. S16. CV at different scan rates from 20 to 160 mV s^{-1} for HER in 1.0 M KOH solution. (a) Ce_{10}/CoFe@C/750, (b) Ce_{20}/CoFe@C/750, (c) Ce_{30}/CoFe@C/750, (d) Ce_{40}/CoFe@C/750, (e) CoFe@C/750, (f) Ce_{20}/CoFe@C/650, and (g) Ce_{20}/CoFe@C/850.

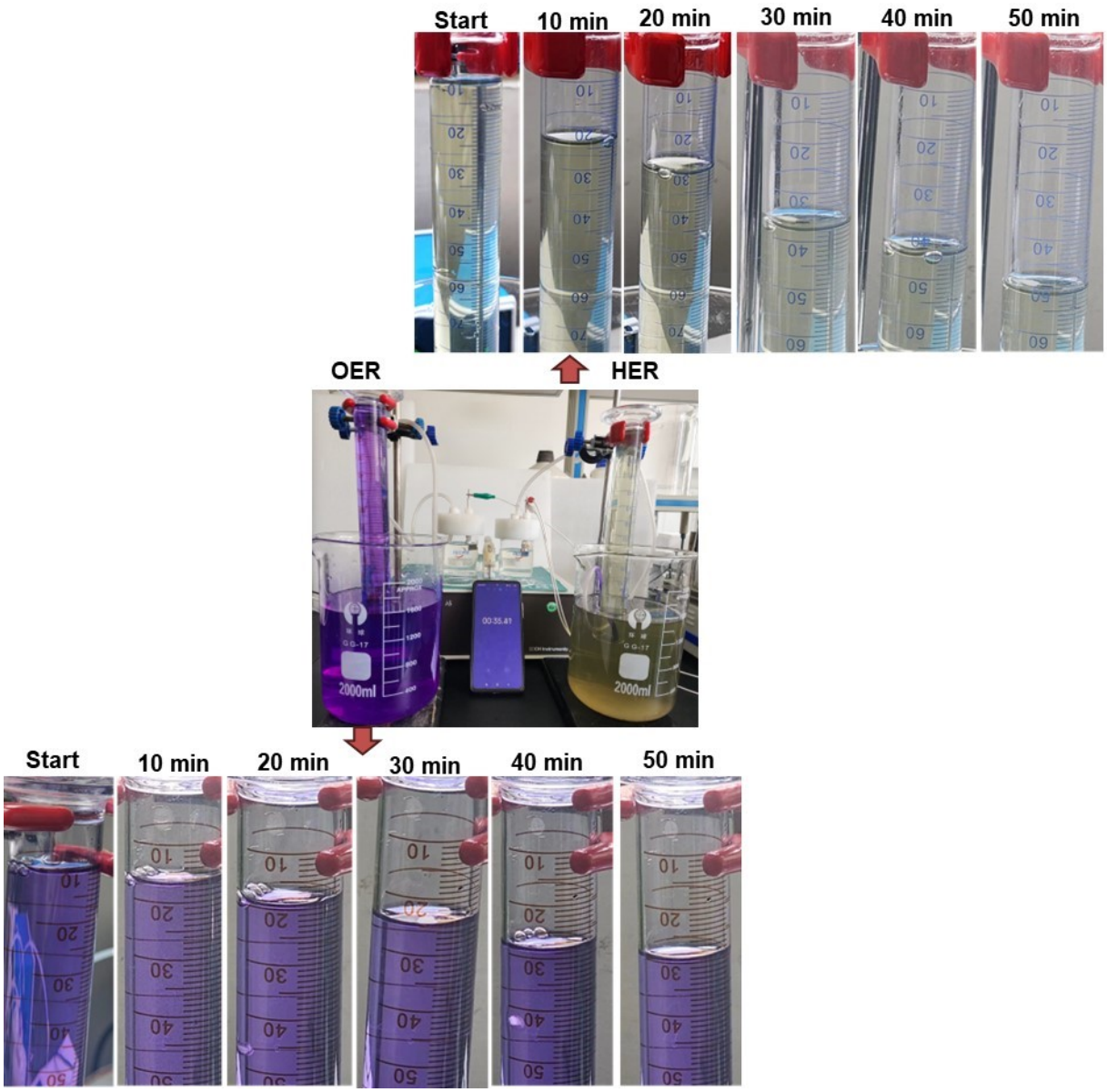

Fig. S17. Measurement of evolved H_2 and O_2 gas volume using a water displacement apparatus.

Table S1. Composition of precursor mixture for CeO_2/CoFe@C catalyst with different Ce content.

Ce (wt%)	Mass of Co salt (g)	Mass of Fe salt (g)	Mass of Ce salt (g)	Mass of Citric Acid (g)	Mass of Tartaric Acid (g)	Total Mass (g)
10	0.166	0.166	0.200	0.733	0.733	2
20	0.166	0.166	0.400	0.633	0.633	2
30	0.166	0.166	0.600	0.533	0.533	2
40	0.166	0.166	0.800	0.433	0.433	2

Table S2: Atomic percentage of different elements calculated from survey data.

Catalyst	Name	Peak Position	FWHM	Area	Atomic %
Ce_{20}/CoFe@C/750	C1s	284.8	1.35	197502.57	80.03
	Ce3d	883.43	7.21	130939.77	1.44
	Co2p	781.38	4.06	61809.98	2.05
	Fe2p	711.82	4.07	61961.53	2.44
	O1s	531.64	3.56	83728.9	14.03
CoFe@C/750	C1s	284.8	1.25	202186.69	81.62
	Co2p	781.3	4.57	75396.22	2.49
	Fe2p	711.97	4.61	69310.07	2.72
	O1s	531.68	3.21	78878.06	13.17

Table S3. Electrochemical performance for OER in 1.0 M KOH electrolyte media.

	Catalyst	Overpotential η_{10} (mV)	Tafel (mV dec^{-1})	C_{dl} (mF cm^{-2})	ECSA (cm^2_{ECSA})
1.	Ce_{10}/CoFe@C/750	244	51.8	22.7	567
2.	Ce_{20}/CoFe@C/750	191	38.8	24.7	617
3.	Ce_{30}/CoFe@C/750	256	62.6	14.5	362
4.	Ce_{40}/CoFe@C/750	283	50.4	11.7	292
5.	CoFe@C/750	298	54.4	10.7	267
6.	RuO_2	324	71.6	-	-
7.	Ce_{20}/CoFe@C/650	270	67.3	13.2	330
8.	Ce_{20}/CoFe@C/850	261	45.3	17.6	440

Table S4. The equivalent circuit diagram fitting values of the electrochemical impedance spectrum for different catalysts.

	R_s (Ω) OER	R_{ct} (Ω) OER	R_s (Ω) HER	R_{ct} (Ω) HER
Ce_{10}/CoFe@C/750	1.292	47.24	1.03	25.8
Ce_{20}/CoFe@C/750	0.05	6.82	1.00	22.4
Ce_{30}/CoFe@C/750	0.87	21.9	0.81	41.4
Ce_{40}/CoFe@C/750	1.87	90.7	0.95	82.8
CoFe@C/750	1.18	157.1	0.86	39.4
Ce_{20}/CoFe@C/650	1.23	72.5	0.56	84.4
Ce_{20}/CoFe@C/850	0.72	46.7	0.45	37.6

Table S5. Electrochemical activity for HER in 1.0 M KOH electrolyte media.

	Catalyst	Overpotential η_{10} (mV)	Tafel (mV dec^{-1})	C_{dl} (mF cm^{-2})	ECSA (cm^2_{ECSA})
1.	Pt/C 10%	56	60.2	-	-
2.	Ce_{10}/CoFe@C/750	147	123.9	19.1	477
3.	Ce_{20}/CoFe@C/750	124	105.3	22.1	552
4.	Ce_{30}/CoFe@C/750	225	129.1	9.45	236
5.	Ce_{40}/CoFe@C/750	215	136.3	8.19	204
6.	CoFe@C/750	201	132.0	10.9	272
7.	Ce_{20}/CoFe@C/650	196	121.2	18.1	452
8.	Ce_{20}/CoFe@C/850	189	115.0	19.8	495

Table S6: The comparative performance of most recently reported literature for HER, OER, and overall water splitting in 1.0 M KOH solution.

Electrocatalyst	Overpotential (η, mV) at 10 mA cm^{-2}		Tafel slope ($mV\ dec^{-1}$)		Overall voltage (V) at 10 mA cm^{-2}	Reference
	HER	OER	HER	OER		
Ce_{20}/CoFe@C/750	114	191	105.3	38.8	1.508	This work
$CeCO_3OH$/Ce-CoFe LDH	165	216	89.8	40.1	1.610	[3]
$Co_{1-\delta}Fe_{\delta}$ LDH/g-CN_x	270	280	79	29	1.610	[4]
CoFe-LDH/GF	-	252	-	61	-	[5]
CoFeO@BP	88	266	51	42	1.58	[6]
Ce-CoFe-LDH/NF	-	225	-	34.3	-	[7]
5% Ce-CoP/Fe2P	-	250	-	46.1	-	[8]
FeO_x/CeO_2	-	252		45	-	[9]
$CeO_2Co_{0.9}Fe_{0.1}$-Se/NF–CoO	-	296	-	76.7	-	[10]
NiCoFeB	174	208	60.2	41.4	1.630	[11]
CoSe-CC/NiSe-CC,	180	420	64.2	59.2	1.600	[12]
$NiMn_2O$@NM	248	250	198	218	1.690	[13]
Cd-Ni_3S_2/NF	140	197	144	54	1.540	[14]
$Co_3Fe/Ce_{0.025}$	178	285	75.3	47.2	1.700	[15]
Co0.9Fe0.1-Se/NF	125	246	85.4		1.550	[16]
Co-Ni-P@NF	92	277	87.6	63.6	1.640	[17]
CoNiP/NF	147	234	51	47	1.620	[18]
NiFe-Pi/P@NF**	97	255	56	81	1.570	[19]
Ni_2P@NPC@CC	92	280	59	48.5	1.540	[20]
Cu@CoFe LDH	171	240	36.4	44.4	1.681	[21]
CoMo@BC	167	279	98.7	67.14	1.650	[22]
Ru-FeCoP	94	310	95.4	62.8	1.650	[23]
Mo_xC/Ni_3Fe@GL	150	265	89.96	59.6	1.523	[24]

References

[1] B. Zhang, X. Zheng, O. Voznyy, R. Comin, M. Bajdich, M. García-Melchor, L. Han, J. Xu, M. Liu, L. Zheng, F.P.G. De Arquer, C.T. Dinh, F. Fan, M. Yuan, E. Yassitepe, N. Chen, T. Regier, P. Liu, Y. Li, P. De Luna, A. Janmohamed, H.L. Xin, H. Yang, A. Vojvodic, E.H. Sargent, Homogeneously dispersed multimetal oxygen-evolving catalysts, Science (80-.). (2016). https://doi.org/10.1126/science.aaf1525.

[2] Z. Yan, H. Sun, X. Chen, H. Liu, Y. Zhao, H. Li, W. Xie, F. Cheng, J. Chen, Anion insertion enhanced electrodeposition of robust metal hydroxide/oxide electrodes for oxygen evolution, Nat. Commun. 9 (2018) 2373. https://doi.org/10.1038/s41467-018-04788-3.

[3] J. Tang, J. Hu, X. Chen, B. Yang, K. Zhang, Y. Li, Y. Yao, S. Zhang, Boosting activity on CoFe layered double hydroxide by doping and heterostructure as a bifunctional electrocatalyst for efficient overall water splitting, Fuel. (2024). https://doi.org/10.1016/j.fuel.2024.131128.

[4] T. Bhowmik, M.K. Kundu, S. Barman, CoFe Layered Double Hydroxide Supported on Graphitic Carbon Nitrides: An Efficient and Durable Bifunctional Electrocatalyst for Oxygen Evolution and Hydrogen Evolution Reactions, ACS Appl. Energy Mater. 1 (2018) 1200–1209. https://doi.org/10.1021/acsaem.7b00305.

[5] B. Deng, J. Liang, L. Yue, T. Li, Q. Liu, Y. Liu, S. Gao, A.A. Alshehri, K.A. Alzahrani, Y. Luo, X. Sun, CoFe-LDH nanowire arrays on graphite felt: A high-performance oxygen evolution electrocatalyst in alkaline media, Chinese Chem. Lett. (2022). https://doi.org/10.1016/j.cclet.2021.10.002.

[6] X. Li, L. Xiao, L. Zhou, Q. Xu, J. Weng, J. Xu, B. Liu, Adaptive Bifunctional Electrocatalyst of Amorphous CoFe Oxide @ 2D Black Phosphorus for Overall Water Splitting, Angew. Chemie - Int. Ed. (2020). https://doi.org/10.1002/anie.202008514.

[7] L. Wang, Y. Liu, X. Liu, W. Chen, 3D nanostructured Ce-doped CoFe-LDH/NF self-supported catalyst for high-performance OER, Dalt. Trans. 52 (2023) 12038–12048. https://doi.org/10.1039/D3DT01814H.

[8] Y. Huang, M. Li, W. Yang, Y. Yu, S. Hao, Ce-Doped Ordered Mesoporous Cobalt Ferrite Phosphides as Robust Catalysts for Water Oxidation, Chem. – A Eur. J. 26 (2020) 13305–13310. https://doi.org/10.1002/chem.202003185.

[9] Q. Sun, Y. Liu, X. Li, X. Guo, W.-H. Huang, Y. Zhu, Z. Wang, C.-C. Chueh, C.-L. Chen, Y.-K. Peng, Z. Zhu, Highly Disordered Fe-Doped CeO 2 with Oxygen Vacancies Facilitates Electrocatalytic Water Oxidation, Energy & Fuels. 37 (2023) 9434–9443. https://doi.org/10.1021/acs.energyfuels.3c00621.

[10] W. Li, L. Zhao, C. Wang, X. Lu, W. Chen, Interface Engineering of Heterogeneous CeO 2 – CoO Nanofibers with Rich Oxygen Vacancies for Enhanced Electrocatalytic Oxygen Evolution Performance, ACS Appl. Mater. Interfaces. 13 (2021) 46998–47009. https://doi.org/10.1021/acsami.1c11101.

[11] M. Moloudi, A. Noori, M.S. Rahmanifar, Y. Shabangoli, M.F. El-Kady, N.B. Mohamed, R.B. Kaner, M.F. Mousavi, Layered Double Hydroxide Templated Synthesis of Amorphous NiCoFeB as a Multifunctional Electrocatalyst for Overall Water Splitting and Rechargeable Zinc–Air Batteries, Adv. Energy Mater. 13 (2023). https://doi.org/10.1002/aenm.202203002.

[12] M. Hassan, M.M. Baig, S. Yousaf, M. Faheem, A. Hussain, B. Niaz, F.A. Khan, S. Aziz, Y. Ahmed, K.H. Shah, S.G. Lee, Efficient water splitting catalyst: Low-temperature selenization of Co and Ni hydroxide nanosheets on carbon cloth for enhanced electro-catalytic activity, Diam. Relat. Mater. 139 (2023) 110298. https://doi.org/10.1016/j.diamond.2023.110298.

[13] P.C. Nagajyothi, K. Pavani, R. Ramaraghavulu, J. Shim, Microwave synthesis of NiMn2O4/Ni-foam: Efficient bifunctional electrocatalysts for overall water splitting, Int. J. Hydrogen Energy. (2023). https://doi.org/10.1016/j.ijhydene.2023.09.046.

[14] H. Yan, R. Deng, S. Zhang, H. Yao, J. Duan, H. Bai, Y. Li, R. Liu, K. Shi, S. Ma, Cd doped Ni3S2 nanosheet arrays grown on nickel foam as highly efficient and robust bifunctional electrocatalysts for alkaline overall water splitting, J. Alloys Compd. 954 (2023) 170072. https://doi.org/10.1016/j.jallcom.2023.170072.

[15] X.-Z. Song, T. Zhang, Y.-H. Zhao, J.-C. Ni, Y. Pan, Z. Tan, X.-F. Wang, Heterostructure Interface Engineering in CoP/FeP/CeO x with a Tailored d-Band Center for Promising Overall Water Splitting Electrocatalysis, Inorg. Chem. 62 (2023) 8347–8356. https://doi.org/10.1021/acs.inorgchem.3c00876.

[16] H. Ren, L. Yu, L. Yang, Z.H. Huang, F. Kang, R. Lv, Efficient electrocatalytic overall water splitting and structural evolution of cobalt iron selenide by one-step electrodeposition, J. Energy Chem. (2021). https://doi.org/10.1016/j.jechem.2021.01.002.

[17] L. Chai, S. Liu, S. Pei, C. Wang, Electrodeposited amorphous cobalt-nickel-phosphide-derived films as catalysts for electrochemical overall water splitting, Chem. Eng. J. 420 (2021) 129686. https://doi.org/10.1016/j.cej.2021.129686.

[18] H. Liu, R. Huang, W. Chen, Y. Zhang, M. Wang, Y. Hu, Y. Zhou, Y. Song, Porous 2D cobalt–nickel phosphide triangular nanowall architecture assembled by 3D microsphere for enhanced overall water splitting, Appl. Surf. Sci. 569 (2021) 150762. https://doi.org/10.1016/j.apsusc.2021.150762.

[19] W. Li, M. Chen, Y. Lu, P. Qi, G. Liu, Y. Zhao, H. Wu, Y. Tang, One-pot electrodeposition synthesis of NiFe-phosphate/phosphide hybrid nanosheet arrays for efficient water splitting, Appl. Surf. Sci. 598 (2022) 153717. https://doi.org/10.1016/j.apsusc.2022.153717.

[20] B. Ma, X. Duan, W. Han, X. Fan, Y. Li, F. Zhang, G. Zhang, W. Peng, Decorated nickel phosphide nanoparticles with nitrogen and phosphorus co-doped porous carbon for enhanced electrochemical water splitting, J. Colloid Interface Sci. 567 (2020) 393–401. https://doi.org/10.1016/j.jcis.2020.02.033.

[21] L. Yu, H. Zhou, J. Sun, F. Qin, D. Luo, L. Xie, F. Yu, J. Bao, Y. Li, Y. Yu, S. Chen, Z. Ren, Hierarchical Cu@CoFe layered double hydroxide core-shell nanoarchitectures as bifunctional electrocatalysts for efficient overall water splitting, Nano Energy. 41 (2017) 327–336. https://doi.org/10.1016/j.nanoen.2017.09.045.

[22] W. Yaseen, S. Meng, W. Li, M. Xie, M. Rafiq, B. Adegbemiga Yusuf, S.A. Shah, I. Khan, J. Xie, Y. Xu, Facile synthesis of CoMoO4/CoMoB/boron-doped carbon nanocomposite as a highly durable bifunctional electrocatalyst for overall water splitting, Int. J. Hydrogen Energy. 51 (2024) 565–577. https://doi.org/10.1016/j.ijhydene.2023.06.315.

[23] L. Zhang, X. Cao, C. Guo, A. Hassan, Y. Zhang, J. Wang, Interface and morphology engineering of Ru-FeCoP hollow nanocages as alkaline electrocatalyst for overall water

splitting, J. Environ. Chem. Eng. 11 (2023) 111373. https://doi.org/https://doi.org/10.1016/j.jece.2023.111373.

[24] P. Zhang, J. Zhang, Y. Fu, J. Zhang, J. Wang, Bottom-up self-assembly strategy to construct ternary Mo C/Ni3Fe@GL as efficient water splitting electrocatalyst, Int. J. Hydrogen Energy. 51 (2024) 1337–1346. https://doi.org/10.1016/j.ijhydene.2023.11.082.